Noname manuscript No.
(will be inserted by the editor)

Genome-based kinetic modeling of cytosolic glucose metabolism in industrially relevant cell lines – *Saccharomyces cerevisiae* and Chinese hamster ovary cells

Ning Chen · Georgios C. Koumpouras · Karen M. Polizzi · Cleo Kontoravdi

Received: date / Accepted: date

Abstract Model-based analysis of cellular metabolism can facilitate our understanding of intracellular kinetics and aid the improvement of cell growth and biological product manufacturing. In this paper, a model-based kinetic study of cytosolic glucose metabolism for two industrially relevant cell lines, *Saccharomyces cerevisiae* and Chinese hamster ovary (CHO) cells, based on enzyme genetic presence and expression information is described. We have reconstructed the cytosolic glucose metabolism map for *S. cerevisiae* and CHO cells, containing 18 metabolites and 18 enzymes using information from the Kyoto Encyclopedia of Genes and Genomes (KEGG). Based on this map, we have developed a kinetic mathematical model for the pathways involved, considering regulation and/or inhibition by products or co-substrates. The values of the maximum rates of reactions (V_{max}) were estimated based on kinetic parameter information and metabolic flux analysis results available in literature and resulting simulation results for steady state metabolite concentrations are

Ning Chen
Centre for Process Systems Engineering, Department of Chemical Engineering and Chemical Technology, Imperial College London, South Kensington Campus, London SW7 2AZ, U.K.

Georgios C. Koumpouras
Department of Consulting, Process Systems Enterprise, London W6 7HA, U.K.

Karen M. Polizzi
Centre for Synthetic Biology and Innovation, Imperial College London, South Kensington Campus, London SW7 2AZ, U.K.
Division of Molecular Biosciences, Department of Life Sciences, Imperial College London, South Kensington Campus, London SW7 2AZ, U.K.

Cleo Kontoravdi
Centre for Process Systems Engineering, Department of Chemical Engineering and Chemical Technology, Imperial College London, South Kensington Campus, London SW7 2AZ, U.K.
Tel.: +44 (0)20 7594 6655
E-mail: cleo.kontoravdi98@imperial.ac.uk

in good agreement with published experimental data. Finally, the model was used to analyse how the production of DHAP, an important intermediate in fine chemicals synthesis, could be increased using gene knockout.

Keywords kinetic modelling · *Saccharomyces cerevisiae* · Chinese hamster ovary cells · genome-scale metabolic reconstruction · glucose metabolism

1 Introduction

Detailed kinetic modelling, which describes all the enzymatic reaction steps, is the most comprehensive way of modelling cellular metabolism. However, the validation of such a modelling approach requires a considerable amount of high quality intracellular data, which are difficult to obtain experimentally and are cell line dependent. Hence, considerable resources are needed to parameterize the model and studies sought alternative methods to model cellular metabolism, *e.g.*, by simplifying the reaction network (*e.g.* [43, 60]), developing models based only on reaction stoichiometry (*e.g.* [49]), or performing metabolic flux analyses (*e.g.* [13, 44]). However, these models do not have the ability to describe the exact intracellular metabolic activity and how this changes over cell culture time or, equally importantly, enzyme regulation by certain metabolites. Hence, even though some regulation effects have been described in detail, to the best of our knowledge there are a limited number of published kinetic studies that examine an entire metabolic network in detail.

Glucose metabolism is essential for cell survival as the preferred cellular supply of energy. However, glucose acts not only as an energy source but also as a carbon skeleton donor for the tricarboxylic acid (TCA) cycle, as well as for nucleic and amino acid synthesis via the pentose phosphate pathway (PPP). The ability to quantitatively describe metabolic activity is essential for analyzing cellular nutrient requirements and hence devising appropriate cell culture media and feeding strategies. Glucose metabolism has been studied in significant detail experimentally, thus rendering the development of a kinetic model for this reaction network a good starting point for modelling cellular metabolism.

In the first structured, kinetic single-cell model for CHO cells [60], a simplified network for 18 metabolic components including amino acid, glucose, lactate, DNA, RNA and proteins, which separated the cell into two compartments, the cytocol and the nucleus, was presented. Sanderson [43] developed a new model that tracked intracellular concentrations, considered competitive amino acid transport, as well as fatty acid and amino acid metabolism, and new cell and product formation algorithms. Following this work, the aforementioned single cell model and a population balance model was coupled [48]. These models simplified the metabolic pathways heavily, for example considering glycolysis as a set of 3 sequential reactions, and lacked the ability to determine the role of lumped metabolites. A recent model for glycolytic oscillations in starved *S. cerevisiae* cell cultures [23] based on detailed enzymatic reactions demonstrates that kinetic modelling of cell metabolism is an

achievable goal and a reasonable method for analysing metabolic behaviour. Importantly, recent genome-scale kinetic studies (*e.g.* [50, 51]) have gained increased research interest and have found application both in the analysis of cell metabolism as well as in the optimisation of bioprocesses.

We have launched a genome-based kinetic study of metabolism in both yeast and mammalian cells starting from cytosolic glucose metabolism, which includes glycolysis and the PPP. Herein, we present a mechanistic model for two industrially-relevant cell lines, *S. cerevisiae* cells, a yeast cell line, and CHO cells, a mammalian cell line with a more complex metabolic network, developed in line with the methodology outlined in [54]. Reaction kinetics were modelled explicitly with a minimum number of reactions lumped due to lack of experimental information, as depicted in Figures 2 and 3. Parameter values for these models were estimated using kinetic information from literature and published MFA studies for the pathways considered. Since various MFA studies report different numerical values for the fluxes of the pathways for the same organism depending on the cell growth phase the measurements were conducted in, we further assessed how significant the resulting differences in estimated parameter values can be. Finally, as an application of the model, we performed a simulation study on enhancing DHAP production by knocking out the gene for triose-phosphate isomerase.

2 Mathematical model development

We built a kinetic model for cytosolic glucose metabolism for *S. cerevisiae* and CHO cells to describe the metabolic map shown in Figure 1 (abbreviations are explained in Tables 1 & 2). The map was constructed based on genetic and kinetic information from two online databases, namely the Kyoto Encyclopedia of Genes and Genomes (KEGG) and the Braunschweig Enzyme Database (BRENDA), respectively. Since complete genomic information on CHO cells is currently not publicly available, we used that of the closest species, *Rattus norvegicus*, as a substitute when required.

Eighteen metabolites and eighteen reactions compose the metabolic map, which includes glycolysis and the pentose-phosphate pathway. The model is a system of ordinary differential and algebraic equations and consists of mass balances for all metabolites and kinetic rates for all enzymatic reactions. Mass balances equations are described as:

$$\frac{\mathrm{d}c_i}{\mathrm{d}t} = \sum_j s_{i,j} v_j + F_{in,i} - F_{out,i}, \tag{1}$$

where $s_{i,j}$ are the stoichiometric coefficients as presented in Table 5 and v_j represent the reaction rates. The rates are described mathematically as summarised in Table 4 using Michaelis-Menten kinetics and account for known regulation (activation and inhibition) effects. Co-factors (NAD^+, NADH, *etc.*) are assumed to be present at sufficient concentrations, and redox metabolism (from NADH to NAD^+) has not been considered in line with previous kinetic

models [19, 26, 42]. $F_{in,i}$ and $F_{out,i}$ are the rates at which metabolite i is fed into and out of the system via side reactions accounting for other metabolic pathways or trans-membrane transport.

Since available enzyme kinetic data are derived from studies performed *in vitro*, only Michaelis-Menten constants K_m can be considered accurate for the purpose of simulating *in vivo* behaviour. The V_{max} values require estimation from experimental findings. Metabolic flux analysis data are only reported as net fluxes, thus it is not possible to consider the reversible reactions in our model. Hence, for the majority of the reactions, only net forward reaction rates are considered, which are described using apparent Michaelis-Menten constants ($K_{m,app}$) and maximum rates of reaction ($V_{max,app}$).

Based on data availability, namely metabolite concentrations (see Table 1) and enzyme kinetic constants (see Table 3 & 4), the metabolic model was reduced by grouping certain adjacent reactions, in order to avoid inaccuracies and overfitting of kinetic parameters. Specifically, for *S. cerevisiae* cells, the concentrations of 1,3-bisphosphoglycerate (13BPG) and 6-phospho-glucono-1,5-lactone (6PGL) in glycolysis, and ribulose-5-phosphate (Ru5P), ribose-5-phosphate (R5P) and xylulose-5-phosphate (X5P) in the PPP have not been reported experimentally, while the concentration of erythrose-4-phosphate (E4P) and sedoheptulose-7-phosphate (S7P) have been reported as non-detectable[46]. Therefore, the reaction catalysed by phosphoglycerate kinase (PGK), which uses 13BPG as a substrate, is grouped with the previous reaction. Moreover, since there is little information for the PPP, the entire pathway has been grouped.

Metabolic flux analysis studies have showed that the metabolic fluxes exiting glycolysis and the PPP are considerable [17, 20, 22, 47] and therefore need to be taken into account in the model. Based on the reconstructed metabolic map and fluxes reported in [20, 22], the set of $F_{in,i}$ and $F_{out,i}$ considered in the model for *S. cerevisiae* are:

(1) $F_{in,\mathrm{Glc}}$, feed of glucose from media via trans-membrane transport,
(2) $F_{out,\mathrm{G6P}}$, reactions towards nucleotide sugar donor metabolism and PPP
(3) $F_{in,\mathrm{F6P}}$, reactions from PPP,
(4) $F_{out,\mathrm{F6P}}$, reactions towards synthesis of fructose 2,6-bisphosphate,
(5) $F_{in,\mathrm{GA3P}}$, reactions from PPP,
(6) $F_{out,\mathrm{GA3P}}$, reactions towards PPP,
(7) $F_{out,\mathrm{DHAP}}$, reactions towards synthesis of glycerol,
(8) $F_{out,\mathrm{13BPG}}$, reactions towards synthesis of amino acids,
(9) $F_{out,\mathrm{Pyr}}$, reactions towards synthesis of lactate, synthesis of amino acids and TCA cycle,

The reduced model based on the above considerations was based on the revised metabolic map shown in Figure 2.

Similarly, for CHO cells, since the concentrations of 13BPG and 6PGL are not available in the literature, these two relevant reactions, namely PGK and PGLS, were grouped with their upstream reactions, GAPDH and G6PDH, respectively. The missing concentration of F26BP was approximated to 0.005 mM

based on experimental findings reported in [57]. Importantly, the model considers the pathways towards other metabolic networks and homeostatic activities, including amino acid and nucleotide sugar donor metabolism, the TCA cycle, DNA synthesis, and lactate and glycerol accumulation, for which experimental information is available. The following inlet and outlet flows were therefore considered in the model for CHO cells:

(1) $F_{in,\mathrm{Glc}}$, feed of glucose from media via trans-membrane transport,
(2) $F_{out,\mathrm{G6P}}$, reactions towards nucleotide sugar donor metabolism,
(3) $F_{out,\mathrm{F6P}}$, reactions towards synthesis of fructose 2,6-bisphosphate,
(4) $F_{out,\mathrm{DHAP}}$, reactions towards synthesis of glycerol,
(5) $F_{out,\mathrm{13BPG}}$, reactions towards synthesis of amino acids,
(6) $F_{out,\mathrm{Pyr}}$, reactions towards the TCA cycle and lactate accumulation,
(7) $F_{out,\mathrm{Ru5P}}$, reactions towards synthesis of DNA and amino acids.

The revised metabolic map based on which the model for CHO cells was developed is shown in Figure 3.

3 Results and Discussion

3.1 Parameter estimation and model simulation

For *S. cerevisiae* cells, various different values for the metabolic flux entering the PPP have been reported, *e.g.*, 2.5%[17], 1.3%-2.8%[47] and 16.2%-44.2%[20]. We have therefore chosen to examine three scenarios. Scenario A uses the metabolic flux distribution reported by Gombert *et al.*[20] for parameter estimation because this is one of the few studies conducted in a defined fermentation medium. This study involved the batch cultivation of *S. cerevisiae* using [1-^{13}C] glucose as the limiting substrate. Samples were removed from the culture at the late exponential phase, were analysed by gas chromatography coupled to mass spectrometry (GC-MS) to measure fractional labelings of intracellular metabolites, and the data were used as inputs to a flux estimation routine. The reported metabolic fluxes were converted herein to units of mM/s using a cell density equal to 1.1029 g/mL[7] and water content of 67%[2] and are presented in Figure 2. Scenario B refers to the estimation results when the metabolic flux towards the PPP in [20] is halved, while scenario C refers to the results obtained when using the experimental results reported by [47]. In all cases, intracellular metabolite concentrations from various sources (see Table 7) were used in conjunction with the aforementioned fluxes for the purpose of parameter estimation.

The apparent V_{max} values for all reactions considered explicitly in the model were estimated in gPROMS (PSE Ltd., U.K.) based on an assumption that net metabolic flux rates equals to counterpart reaction rates, using the metabolite concentrations in Table 1, metabolic fluxes results in Figure 2 and the enzyme kinetics in Table 4. The results for all three cases are presented in Figure 4. Interestingly, the estimated values for all scenarios are comparable. Table 6 summarises the numerical results of the estimation and in most

cases the deviation is within 5%, i.e. within the margin of experimental error. Significant deviation occurs in the case of the V_{max} for GPI, the enzyme that catalyses the conversion of glucose-6-phosphate to fructose-6-phosphate, for which the values under scenarios B and C differ from that for scenario A by 10% and 19.72%, respectively. This result is unsurprising since by reducing the flux to the PPP, an increased glucose flux will be channeled to the main glycolytic pathway for the same glucose utilisation rate. Similarly, this increases the V_{max} for PFK1 and ALD, which catalyse the following two reactions in glycolysis. However, the effect of reduced PPP flux changes the V_{max} values for the remaining enzymes in opposite ways, with values increasing under scenario B and decreasing under scenario C. This can be attributed to the fact that although all fluxes associated with the PPP are lower in scenario C than in other cases, there is a significant increase in the outward fluxes from dihydroxyacetone phosphate (DHAP) towards glycerol, from phosphoenolpyruvate towards the TCA cycle and amino acid metabolism and from pyruvate towards the TCA cycle, amino acid metabolism, and lactate. This significantly affects our estimates for V_{max} in the latter reactions of the glycolytic pathway. This exercise illustrates that a significant impediment in the accurate estimation of kinetic parameters in the lack of complete experimental datasets containing both flux and metabolite concentration information.

Similarly, metabolic fluxes as presented in [22] were used for the estimation of apparent V_{max} values in CHO cells. This study involved the quantification of steady state isotopomer distribution in a perfusion bioreactor operated with 10% [U-^{13}C] glucose, 40% labelled [1-^{13}C] glucose and 50% unlabelled glucose, from which metabolic fluxes were determined using the 13C-Flux software package. The fluxes were converted to mM/s from $pmol/cell \cdot day$ reported in Goudar's work [22] using a CHO cell diameter equal to 15 μm[24]. The converted metabolic flux values, which were used for parameter estimation herein, are presented in Figure 3. Again, intracellular metabolite concentrations from [1] and [41] (see Table 7 for values) were used in tandem with the aforementioned fluxes for the estimation of unknown parameter values.

The estimated values for CHO are presented in Figure 4 and 5. The estimated apparent values of V_{max} for the first four enzymes in glycolysis, namely GCK, PGI, PFK1 and ALD, are considerably lower than for those enzymes from the latter part of glycolysis, namely GAPDH, PGM, ENO and PK. Our findings suggest that the rate of glycolysis is mostly limited by earlier reactions in both *S. cerevisiae* and CHO cells. As presented in Table 7, the steady-state simulation results are in agreement with known metabolite concentrations for both cell lines. Where a range of values was available from literature, the parameter estimation was carried out to minimise the difference between simulation results and the lower value reported, hence, the agreement with this value is reported.

3.2 DHAP production analysis

DHAP is an important metabolite and intermediate in the synthesis of fine chemicals. We therefore sought to analyse how the cell-based production of DHAP in *S. cerevisiae* can be improved. As shown in the metabolic map (Figure) and the flux distribution in Figure , DHAP is one of the two products of the reaction catalysed by ALD together with glyceraldehyde 3-phosphate (GA3P). It is also the substrate of the reversible reaction catalysed by TPI towards GA3P. From the network structure, it is deduced that one strategy for increasing the production rate of DHAP would be by knocking out the gene for TPI, as attempted in the cell-free study described in [8]. This was simulated for *S. cerevisiae* by setting the value for $V_{max,\mathrm{TPI}}$ equal to zero in the mathematical model. Following this, the glucose uptake rate, q_{Glc} was varied between 0.1 μM and 20 μM (approximately twice the value reported in [20]) and the system was simulated until it reached steady-state. Two outputs, namely the steady-state DHAP accumulation rate $\delta\mathrm{DHAP}/\delta t$ and yield of DHAP over Glucose $Y_{\mathrm{DHAP,Glc}}$, were recorded and are shown in Figure 6. At about $q_{\mathrm{Glc}} = 0.0155\ mM/s$, $\delta\mathrm{DHAP}/\delta t$ stops increasing because of the limitation of the low V_{max} values in the early part of glycolysis while $Y_{\mathrm{DHAP,Glc}}$ reaches the peak. This value is 28% bigger than the flux in Figure 2, which shows that *S. cerevisiae* metabolism is not operating at a very efficient state, and there are about 28% for increasing. Our findings also showed that there is no significant difference in fluxes and metabolite concentration in the early part of glycolysis and PPP under different glucose uptake rates in the presence and absence of TPI (data not included), which is mainly caused by the omission of rates for the backward reactions (gluconeogenesis)in glycolysis.

4 Conclusions

Kinetic modelling is a demanding yet powerful method to study cellular metabolism and related bioprocessing applications. Herein, we examined how it can be applied to analyse extracellular culture data for two commonly used cell lines. We additionally demonstrated its potential usefulness for analysing genetic manipulation effects and evaluating process operation conditions. When coupled with meaningful experiments, kinetic modelling can therefore facilitate our understanding of regulation effects and help optimize cell culture conditions. However, considerable computational and experimental work is still required to enrich related enzyme databases.

First, a more complete map for glucose metabolism needs to be considered including hexose phosphate(s), *e.g.*, F1P and F26BP, and the metabolic pathway towards glycerol, which are important in glycolysis inhibition/activation and metabolite generation. Second, informative cell culture experiments can be designed specifically for parameter estimation and model validation, as demonstrated in [28]. Specifically, isotope labelling can be employed to determine the concentrations of individual metabolites as a function of cell culture

time. The collection of high-quality dynamic data on extracellular and intracellular metabolite concentrations, in conjunction with a transcriptomic analysis on the metabolic enzymes, can enable the accurate determination of the kinetic properties of each enzyme involved using model-based network analysis. Once such a kinetic model has been developed and validated it will become possible to use it in order to optimize the cell culture process and media formulation based on an advanced understanding of the contribution of all metabolites and enzymes.

Acknowledgements The authors thank Alireza Behjousiar for his kind help with experimentation and Ioscani Jiménez del Val for his kind help with gPROMS. Financial support from the Centre for Process Systems Engineering Industrial Consortium is gratefully acknowledged. Finally, CK would like to thank Research Councils UK and Lonza Biologics plc for her fellowship.

References

1. Albe KR, Butler MH, Wright BE (1990) Cellular concentrations of enzymes and their substrates. J Theor Biol 143(2):163–195
2. Alcázar E, Rocha-Leão M, Dweck J (2000) Yeast intracellular water determination by thermogravimetry. Journal of Thermal Analysis and Calorimetry 59(3):643–648
3. Aust A, Yun SL, Suelter CH (1975) Pyruvate kinase from yeast (saccharomyces cerevisiae). Methods Enzymol 42:176–182
4. Bär J, Naumann M, Reuter R, Kopperschläger G (1996) Improved purification of ribulose 5-phosphate 3-epimerase from saccharomyces cerevisiae and characterization of the enzyme. Bioseparation 6(4):233–241
5. Blass JP, Piacentini S, Boldizsar E, Baker A (1982) Kinetic studies of mouse brain transketolase. J Neurochem 39(3):729–733
6. Bloch W, MacQuarrie RA, Bernhard SA (1971) The nucleotide and acyl group content of native rabbit muscle glyceraldehyde 3-phosphate dehydrogenase. J Biol Chem 246(3):780–790
7. Bryan AK, Goranov A, Amon A, Manalis SR (2010) Measurement of mass, density, and volume during the cell cycle of yeast. Proc Natl Acad Sci U S A 107(3):999–1004
8. Bujara M, Schmperli M, Billerbeck S, Heinemann M, Panke S (2010) Exploiting cell-free systems: Implementation and debugging of a system of biotransformations. Biotechnol Bioeng 106(3):376–389
9. Byers LD (1982) Glyceraldehyde-3-phosphate dehydrogenase from yeast. Methods Enzymol 89 Pt D:326–335
10. Corpas FJ, García-Salguero L, Barroso JB, Aranda F, nez JAL (1995) Kinetic properties of hexose-monophosphate dehydrogenases. ii. isolation and partial purification of 6-phosphogluconate dehydrogenase from rat liver and kidney cortex. Mol Cell Biochem 144(2):97–104
11. Corpas FJ, García-Salguero L, Peragón J, Lupiáñez JA (1995) Kinetic properties of hexose-monophosphate dehydrogenases. i. isolation and par-

tial purification of glucose-6-phosphate dehydrogenase from rat liver and kidney cortex. Life Sci 56(3):179–189
12. de Atauri P, Repiso A, Oliva B, Vives-Corrons JL, Climent F, Carreras J (2005) Characterization of the first described mutation of human red blood cell phosphoglycerate mutase. Biochim Biophys Acta 1740(3):403–410
13. Dorka P, Fischer C, Budman H, Scharer JM (2009) Metabolic flux-based modeling of mab production during batch and fed-batch operations. Bioprocess Biosyst Eng 32(2):183–196
14. Feksa LR, Cornelio A, Dutra-Filho CS, de Souza Wyse AT, Wajner M, Wannmacher CMD (2005) The effects of the interactions between amino acids on pyruvate kinase activity from the brain cortex of young rats. Int J Dev Neurosci 23(6):509–514
15. Fonvielle M, Coinçon M, Daher R, Desbenoit N, Kosieradzka K, Barilone N, Gicquel B, Sygusch J, Jackson M, Therisod M (2008) Synthesis and biochemical evaluation of selective inhibitors of class ii fructose bisphosphate aldolases: towards new synthetic antibiotics. Chemistry 14(28):8521–8529
16. Gancedo JM, Gancedo C (1973) Concentrations of intermediary metabolites in yeast. Biochimie 55(2):205–211
17. Gancedo JM, Lagunas R (1973) Contribution of the pentose-phosphate pathway to glucose metabolism in Saccharomyces cerevisiae: A critical analysis on the use of labelled glucose. Plant Sci Lett 1:193–200
18. Gao H, Leary JA (2003) Multiplex inhibitor screening and kinetic constant determinations for yeast hexokinase using mass spectrometry based assays. J Am Soc Mass Spectrom 14(3):173–181
19. Gao J, Gorenflo VM, Scharer JM, Budman HM (2007) Dynamic metabolic modeling for a mab bioprocess. Biotechnol Prog 23(1):168–181
20. Gombert AK, Moreira dos Santos M, Christensen B, Nielsen J (2001) Network identification and flux quantification in the central metabolism of Saccharomyces cerevisiae under different conditions of glucose repression. J Bacteriol 183(4):1441–1451
21. González-Mondragón E, Zubillaga RA, Saavedra E, Chánez-Cárdenas ME, Pérez-Montfort R, Hernández-Arana A (2004) Conserved cysteine 126 in triosephosphate isomerase is required not for enzymatic activity but for proper folding and stability. Biochemistry 43(11):3255–3263
22. Goudar C, Biener R, Boisart C, Heidemann R, Piret J, de Graaf A, Konstantinov K (2010) Metabolic flux analysis of CHO cells in perfusion culture by metabolite balancing and 2D [13C, 1H] COSY NMR spectroscopy. Metab Eng 12(2):138–149
23. Hald BO, Sørensen PG (2010) Modeling diauxic glycolytic oscillations in yeast. Biophys J 99(10):3191–3199
24. Han Y, Liu XM, Liu H, Li SC, Wu BC, Ye LL, Wang QW, Chen ZL (2006) Cultivation of recombinant chinese hamster ovary cells grown as suspended aggregates in stirred vessels. J Biosci Bioeng 102(5):430–435
25. He W, Wang Y, Liu W, Zhou CZ (2007) Crystal structure of Saccharomyces cerevisiae 6-phosphogluconate dehydrogenase Gnd1. BMC Struct Biol 7:38

26. Hjersted JL, Henson MA (2006) Optimization of fed-batch saccharomyces cerevisiae fermentation using dynamic flux balance models. Biotechnol Prog 22(5):1239–1248
27. Kiely ME, Stuart AL, Wood T (1973) Partial purification and kinetic properties of ribose-5-phosphate ketol-isomerase and ribulose-5-phosphate 3-epimerase from various sources. Biochim Biophys Acta 293(2):534–541
28. Kontoravdi C, Pistikopoulos EN, Mantalaris A (2010) Systematic development of predictive mathematical models for animal cell cultures. Comput Chem Eng 34(8):1192–1198
29. Krietsch WK, Pentchev PG, Klingenbürg H, Hofstätter T, Bücher T (1970) The isolation and crystallization of yeast and rabbit liver triose phosphate isomerase and a comparative characterization with the rabbit muscle enzyme. Eur J Biochem 14(2):289–300
30. Kusakabe T, Motoki K, Hori K (1994) Human aldolase C: Characterization of the recombinant enzyme expressed in Escherichia coli. J Biochem 115(6):1172–1177
31. Lagunas R, Gancedo C (1983) Role of phosphate in the regulation of the Pasteur effect in Saccharomyces cerevisiae. Eur J Biochem 137(3):479–483
32. Lambeir AM, Opperdoes FR, Wierenga RK (1987) Kinetic properties of triose-phosphate isomerase from trypanosoma brucei brucei. a comparison with the rabbit muscle and yeast enzymes. Eur J Biochem 168(1):69–74
33. Lindell TJ, Stellwagen E (1968) Purification and properties of phosphofructokinase from yeast. J Biol Chem 243(5):907–912
34. Milewski S, Janiak A, Wojciechowski M (2006) Structural analogues of reactive intermediates as inhibitors of glucosamine-6-phosphate synthase and phosphoglucose isomerase. Arch Biochem Biophys 450(1):39–49
35. Nicolau J, Souza DN, Nunez-Burgos G (2000) Regulation of phosphofructokinase-1 on submandibular salivary glands of rats after isoproterenol administration. Arch Physiol Biochem 108(5):437–443
36. Noltmann E (1972) Aldose-ketose isomerases. In: Boyer P (ed) The Enzymes, vol 6, Acad. Press, New York, pp 271–354
37. Ottaway JH, Mowbray J (1977) The role of compartmentation in the control of glycolysis. Curr Top Cell Regul 12:107–208
38. Patra S, Ghosh S, Bera S, Roy A, Ray S, Ray M (2009) Molecular characterization of tumor associated glyceraldehyde-3-phosphate dehydrogenase. Biochemistry (Moscow) 74(7):717–727
39. Poyner RR, Laughlin LT, Sowa GA, Reed GH (1996) Toward identification of acid/base catalysts in the active site of enolase: comparison of the properties of k345a, e168q, and e211q variants. Biochemistry 35(5):1692–1699
40. Rider CC, Taylor CB (1974) Enolase isoenzymes in rat tissues. electrophoretic, chromatographic, immunological and kinetic properties. Biochim Biophys Acta 365(1):285–300
41. Sabate L, Franco R, Canela EI, Centelles JJ, Cascante M (1995) A model of the pentose phosphate pathway in rat liver cells. Mol Cell Biochem 142(1):9–17

42. Sainz J, Pizarro F, Pérez-Correa JR, Agosin E (2003) Modeling of yeast metabolism and process dynamics in batch fermentation. Biotechnol Bioeng 81(7):818–828
43. Sanderson C (1997) The development and application of a stuctured model for animal cell metabolism. PhD thesis, University of Sydney
44. Sauer U, Hatzimanikatis V, Bailey JE, Hochuli M, Szyperski T, Wüthrich K (1997) Metabolic fluxes in riboflavin-producing Bacillus subtilis. Nat Biotechnol 15(5):448–452
45. Schenk G, Duggleby RG, Nixon PF (1998) Properties and functions of the thiamin diphosphate dependent enzyme transketolase. Int J Biochem Cell Biol 30(12):1297–1318
46. Senac T, Hahn-Hägerdal B (1990) Intermediary metabolite concentrations in xylulose- and glucose-fermenting Saccharomyces cerevisiae cells. Appl Environ Microbiol 56(1):120–126
47. Shen Y, Zhao XQ, Ge XM, Bai FW (2009) Metabolic flux and cell cycle analysis indicating new mechanism underlying process oscillation in continuous ethanol fermentation with saccharomyces cerevisiae under vhg conditions. Biotechnol Adv 27(6):1118–1123
48. Sidoli FR, Mantalaris A, Asprey SP (2005) Toward global parametric estimability of a large-scale kinetic single-cell model for mammalian cell cultures. Ind Eng Chem Res 44(4):868–878
49. Smallbone K, Simeonidis E, Broomhead DS, Kell DB (2007) Something from nothing: bridging the gap between constraint-based and kinetic modelling. FEBS J 274(21):5576–5585
50. Smallbone K, Simeonidis E, Swainston N, Mendes P (2010) Towards a genome-scale kinetic model of cellular metabolism. BMC Syst Biol 4:6
51. Sohn SB, Graf AB, Kim TY, Gasser B, Maurer M, Ferrer P, Mattanovich D, Lee SY (2010) Genome-scale metabolic model of methylotrophic yeast pichia pastoris and its use for in silico analysis of heterologous protein production. Biotechnol J 5(7):705–715
52. Sprenger GA, Schörken U, Sprenger G, Sahm H (1995) Transketolase A of Escherichia coli K12. purification and properties of the enzyme from recombinant strains. Eur J Biochem 230(2):525–532
53. Teusink B, Diderich JA, Westerhoff HV, van Dam K, Walsh MC (1998) Intracellular glucose concentration in derepressed yeast cells consuming glucose is high enough to reduce the glucose transport rate by 50Bacteriol 180(3):556–562
54. Thiele I, Palsson BØ (2010) A protocol for generating a high-quality genome-scale metabolic reconstruction. Nat Protoc 5(1):93–121
55. Toews CJ (1966) Kinetic studies with skeletal-muscle hexokinase. Biochem J 100(3):739–744
56. Tsolas B O; Horecker (1972) Transaldolase. In: Boyer P (ed) The Enzymes, vol 7, Acad. Press, New York, pp 259–280
57. Uyeda K, Furuya E, Luby LJ (1981) The effect of natural and synthetic D-fructose 2,6-bisphosphate on the regulatory kinetic properties of liver and muscle phosphofructokinases. J Biol Chem 256(16):8394–8399

58. White MF, Fothergill-Gilmore LA (1990) Mutase versus synthase: the phosphoglycerate mutase family studied by protein engineering. Biochem Soc Trans 18(2):257
59. Wood T (1979) Purification and properties of d-ribulose-5-phosphate 3-epimerase from calf liver. Biochim Biophys Acta 570(2):352–362
60. Wu P, Ray NG, Shuler ML (1992) A single-cell model for CHO cells. Ann N Y Acad Sci 665(Biochemical Engineering VII: Cellular and Reactor Engineering):152–187
61. Zalitis J, Oliver IT (1967) Inhibition of glucose phosphate isomerase by metabolic intermediates of fructose. Biochem J 102(3):753–759

Table 1 Metabolites abbreviation and concentrations reported experimentally

Abbr.	Metabolite	Concentrations (mM)	
		S. cerevisiae cells	CHO cells
13BPG	1,3-bisphosphoglycerate	-	-
2PG	2-phosphoglycerate	0.420-1.100[37]	0.005[1]
3PG	3-phosphoglycerate	0.100-0.260[37]	0.040-0.048[1]
6PG	6-phospho-gluconate	0.100-0.300[16]	0.018[41]
6PGL	6-phospho-glucono-1,5-lactone	-	-
DHAP	Dihydroxyacetone phosphate	0.330[31]	0.040-0.046[1]
E4P	Erythrose 4-phosphate	Not detectable[46]	0.004[41]
F16BP	Fructose 1,6-phosphate	1.700-4.500[16, 31]	0.046[1]
F26BP	Fructose 2,6-bisphosphate	0.0012[31]	0-0.006[57]
F6P	Fructose 6-phosphate	0.650[1]	0.362[1]
G6P	Glucose 6-phosphate	2.300[31]	1.033[1]
GA3P	Glyceraldehyde 3-phosphate	0.400-1.200[37]	0.021[6]
Glc	Glucose	1.500[53]	2.377[1]
PEP	Phosphoenolpyruvate	$\leq$0.030[16, 31]	0.008[1]
Pyr	Pyruvate	1.600[31]	0.056[1]
R5P	Ribose 5-phosphate	-	0.009[41]
Ru5P	Ribulose 5-phosphate	-	0.012[41]
S7P	Sedoheptulose 7-phosphate	Not detectable[46]	0.068[41]
X5P	Xylulose 5-phosphate	-	0.018[41]
ATP	Adenosine triphosphate	1.100-1.900[16, 31]	3.075[1]
ADP	Adenosine diphosphate	0.320-1.300[16, 31]	1.059[1]
P_i	Phosphate	22.000[31]	5.500[1]

Table 2 Enzymes abbreviations

Abbr.	Enzyme
ALD	Fructose-bisphosphate aldolase
ENO	Phosphopyruvate hydratase
FBP1	Fructose-bisphosphatase
G6PD	Glucose-6-phosphate dehydrogenase
GAPDH	Glyceraldehyde-3-phosphate dehydrogenase
GCK	Glucokinase
G6Pase	Glucose-6-phosphatase
GPI	Glucose-6-phosphate isomerase
HK	Hexokinase
PFK1	6-phosphofructokinase
PGD	Phosphogluconate dehydrogenase
PGK	Phosphoglycerate kinase
PGL	6-phosphogluconolactonase
PGM	Phosphoglycerate mutase
PK	Pyruvate kinase
PPE	Ribulose-phosphate 3-epimerase
RPI	Ribose-5-phosphate isomerase
TA	Transaldolase
TK	Transketolase
TPI	Triose-phosphate isomerase

Table 3 Kinetic reaction rate expression for *S. cerevisiae* cells

Reaction	Kinetic expression	Parameters
HK	$v_{\mathrm{HK}} = \frac{V_{max,\mathrm{HK}}}{\left(1+\frac{K^{\mathrm{Glc}}_{m,\mathrm{HK}}}{[\mathrm{Glc}]}\right)\left[1+\frac{K^{\mathrm{ATP}}_{m,\mathrm{HK}}}{[\mathrm{ATP}]}\left(1+\frac{[\mathrm{ADP}]}{K^{\mathrm{ADP}}_{i,\mathrm{HK}}}\right)\right]}$	$K^{\mathrm{Glc}}_{m,\mathrm{HK}} = 0.13\ mM$[18], $K^{\mathrm{ATP}}_{m,\mathrm{HK}} = 0.10\ mM$[18], $K^{\mathrm{ADP}}_{i,\mathrm{HK}} = 0.122\ mM$ [18]
GPI	$v_{\mathrm{GPI}} = \frac{V_{max,\mathrm{GPI}}}{1+\frac{K^{\mathrm{G6P}}_{m,\mathrm{GPI}}}{[\mathrm{G6P}]}\left(1+\frac{[\mathrm{F6P}]}{K^{\mathrm{F6P}}_{i,\mathrm{GPI}}}\right)}$	$K^{\mathrm{G6P}}_{m,\mathrm{GPI}} = 0.700\ mM$[34], $K^{\mathrm{F6P}}_{i,\mathrm{GPI}} = 0.040\ mM$[34]
PFK1	$v_{\mathrm{PFK1}} = \frac{V_{max,\mathrm{PFK1}}}{\left(1+\frac{K^{\mathrm{F6P}}_{m,\mathrm{PFK1}}}{[\mathrm{F6P}]}\right)\left(1+\frac{K^{\mathrm{ATP}}_{m,\mathrm{PFK1}}}{[\mathrm{ATP}]}\right)}$	$K^{\mathrm{F6P}}_{m,\mathrm{PFK1}} = 0.58\ mM$[33], $K^{\mathrm{ATP}}_{m,\mathrm{PFK1}} = 0.033\ mM$[33]
ALD	$v_{\mathrm{ALD}} = \frac{V_{max,\mathrm{ALD}}}{1+\frac{K^{\mathrm{F16BP}}_{m,\mathrm{ALD}}}{[\mathrm{F16BP}]}}$	$K^{\mathrm{F16BP}}_{m,\mathrm{ALD}} = 0.45\ mM$[15]
TPI	$v_{\mathrm{TPI}} = \frac{V_{max,\mathrm{TPI}}}{1+\frac{K^{\mathrm{DHAP}}_{m,\mathrm{TPI}}}{[\mathrm{DHAP}]}} - \frac{V_{max,r,\mathrm{TPI}}}{1+\frac{K^{\mathrm{GA3P}}_{m,\mathrm{TPI}}}{[\mathrm{GA3P}]}}$	$K^{\mathrm{GA3P}}_{m,\mathrm{TPI}} = 1.1\ mM$[21], $K^{\mathrm{DHAP}}_{m,\mathrm{TPI}} = 2.1\ mM$[21], $K_{cat} = 4.7\ s^{-1}$[21], $K_{cat,r} = 0.5\ s^{-1}$[21]
GADPH	$v_{\mathrm{GADPH}} = \frac{V_{max,\mathrm{GADPH}}}{1+\frac{K^{\mathrm{GA3P}}_{m,\mathrm{GADPH}}}{[\mathrm{GA3P}]}}$	$K^{\mathrm{GA3P}}_{m,\mathrm{GADPH}} = 0.6\ mM$[9]
PGM	$v_{\mathrm{PGM}} = \frac{V_{max,\mathrm{PGM}}}{1+\frac{K^{\mathrm{3PG}}_{m,\mathrm{PGM}}}{[\mathrm{3PG}]}}$	$K^{\mathrm{3PG}}_{m,\mathrm{PGM}} = 0.65\ mM$[58]
ENO	$v_{\mathrm{ENO}} = \frac{V_{max,\mathrm{ENO}}}{1+\frac{K^{\mathrm{2PG}}_{m,\mathrm{ENO}}}{[\mathrm{2PG}]}}$	$K^{\mathrm{2PG}}_{m,\mathrm{ENO}} = 0.3\ mM$[39]
PK	$v_{\mathrm{PK}} = \frac{V_{max,\mathrm{PK}}}{\left(1+\frac{K^{\mathrm{PEP}}_{m,\mathrm{PK}}}{[\mathrm{PEP}]}\right)\left(1+\frac{K^{\mathrm{ADP}}_{m,\mathrm{PK}}}{[\mathrm{ADP}]}\right)}$	$K^{\mathrm{PEP}}_{m,\mathrm{PK}} = 0.099\ mM$[3], $K^{\mathrm{ADP}}_{m,\mathrm{PK}} = 0.16\ mM$[3]
PGD	$v_{\mathrm{PGD}} = \frac{V_{max,\mathrm{PGD}}}{1+\frac{K^{\mathrm{6PG}}_{m,\mathrm{PGD}}}{[\mathrm{6PG}]}}$	$K^{\mathrm{6PG}}_{m,\mathrm{PGD}} = 0.0509\ mM$[25]
PPE	$v_{\mathrm{PPE}} = \frac{V_{max,\mathrm{PPE}}}{1+\frac{K^{\mathrm{Ru5P}}_{m,\mathrm{PPE}}}{[\mathrm{Ru5P}]}}$	$K^{\mathrm{Ru5P}}_{m,\mathrm{PPE}} = 1.5\ mM$[4]
RPI	$v_{\mathrm{RPI}} = \frac{V_{max,\mathrm{RPI}}}{1+\frac{K^{\mathrm{Ru5P}}_{m,\mathrm{RPI}}}{[\mathrm{Ru5P}]}}$	$K^{\mathrm{Ru5P}}_{m,\mathrm{RPI}} = 0.74\ mM$[36]
TK1	$v_{\mathrm{TK1}} = \frac{V_{max,\mathrm{TK1}}}{\left(1+\frac{K^{\mathrm{X5P}}_{m,\mathrm{TK}}}{[\mathrm{X5P}]}\right)\left(1+\frac{K^{\mathrm{R5P}}_{m,\mathrm{TK}}}{[\mathrm{R5P}]}\right)}$	$K^{\mathrm{R5P}}_{m,\mathrm{TK}} = 0.4\ mM$[45], $K^{\mathrm{X5P}}_{m,\mathrm{TK}} = 0.21\ mM$[45]
TK2	$v_{\mathrm{TK2}} = \frac{V_{max,\mathrm{TK2}}}{\left(1+\frac{K^{\mathrm{X5P}}_{m,\mathrm{TK}}}{[\mathrm{X5P}]}\right)\left(1+\frac{K^{\mathrm{E4P}}_{m,\mathrm{TK}}}{[\mathrm{E4P}]}\right)}$	$K^{\mathrm{X5P}}_{m,\mathrm{TK}} = 0.21\ mM$[45], $K^{\mathrm{E4P}}_{m,\mathrm{TK}} = 0.09\ mM$[45]
TA	$v_{\mathrm{TA}} = \frac{V_{max,\mathrm{TA}}}{\left(1+\frac{K^{\mathrm{S7P}}_{m,\mathrm{TA}}}{[\mathrm{S7P}]}\right)\left(1+\frac{K^{\mathrm{GA3P}}_{m,\mathrm{TA}}}{[\mathrm{GA3P}]}\right)}$	$K^{\mathrm{S7P}}_{m,\mathrm{TA}} = 0.18\ mM$[56], $K^{\mathrm{GA3P}}_{m,\mathrm{TA}} = 0.22\ mM$[56]

Table 4 Kinetic reaction rate expressions for CHO cells

Reaction	Kinetic expression	Parameters
HK	$v_{\mathrm{HK}} = \frac{V_{max,\mathrm{HK}}}{\left(1+\frac{K^{\mathrm{Glc}}_{m,\mathrm{HK}}}{[\mathrm{Glc}]}\right)\left(1+\frac{K^{\mathrm{ATP}}_{m,\mathrm{HK}}}{[\mathrm{ATP}]}\right)\left(1+\frac{[\mathrm{G6P}]}{K^{\mathrm{G6P}}_{i,\mathrm{HK}}}\right)}$	$K^{\mathrm{Glc}}_{m,\mathrm{HK}} = 0.11\ mM$ [55], $K^{\mathrm{ATP}}_{m,\mathrm{HK}} = 0.8\ mM$ [55], $K^{\mathrm{G6P}}_{i,\mathrm{HK}} = 9.1\ mM$ [41]
GPI	$v_{\mathrm{GPI}} = \frac{V_{max,\mathrm{GPI}}}{1+\frac{K^{\mathrm{G6P}}_{m,\mathrm{GPI}}}{[\mathrm{G6P}]}}$	$K^{\mathrm{G6P}}_{m,\mathrm{GPI}} = 0.705\ mM$ [61]
PFK1	$v_{\mathrm{PFK1}} = \frac{V_{max,\mathrm{PFK1}}}{\left[(]1+\left(\frac{K^{\mathrm{F6P}}_{m,\mathrm{PFK1}}}{[\mathrm{F6P}]}\right)^{n}\right]\left(1+\frac{K^{\mathrm{ATP}}_{m,\mathrm{PFK1}}}{[\mathrm{ATP}]}\right)}$	$K^{\mathrm{F6P}}_{m,\mathrm{PFK1}} = a[\mathrm{F26BP}] + b$, $n = c[\mathrm{F26BP}] + d$, $a = -164.9\ s^{-1}$, $b = 1.306\ mM/s$, $c = -161.7\ mM^{-1}$, $d = 2.964$ (calculated based on [57]), $K^{\mathrm{ATP}}_{m,\mathrm{PFK1}} = 0.06$[35]
ALD	$v_{\mathrm{ALD}} = \frac{V_{max,\mathrm{ALD}}}{1+\frac{K^{\mathrm{F16BP}}_{m,\mathrm{ALD}}}{[\mathrm{F16BP}]}}$	$K^{\mathrm{F16BP}}_{m,\mathrm{ALD}} = 0.013\ mM$[30]
TPI	$v_{\mathrm{TPI}} = \frac{V_{max,\mathrm{TPI}}}{1+\frac{K^{\mathrm{DHAP}}_{m,\mathrm{TPI}}}{[\mathrm{DHAP}]}\left(1+\frac{[\mathrm{PEP}]}{K^{\mathrm{PEP}}_{i,\mathrm{TPI}}}\right)\left(1+\frac{[\mathrm{3PG}]}{K^{\mathrm{3PG}}_{i,\mathrm{TPI}}}\right)\left(1+\frac{[\mathrm{2PG}]}{K^{\mathrm{2PG}}_{i,\mathrm{TPI}}}\right)} - \frac{V_{max,r,\mathrm{TPI}}}{1+\frac{K^{\mathrm{GA3P}}_{m,\mathrm{TPI}}}{[\mathrm{GA3P}]}\left(1+\frac{[\mathrm{PEP}]}{K^{\mathrm{PEP}}_{i}}\right)\left(1+\frac{[\mathrm{3PG}]}{K^{\mathrm{3PG}}_{i,\mathrm{TPI}}}\right)\left(1+\frac{[\mathrm{2PG}]}{K^{\mathrm{2PG}}_{i,\mathrm{TPI}}}\right)}$	$K^{\mathrm{GA3P}}_{m,\mathrm{TPI}} = 0.32\ mM$ [29], $K^{\mathrm{DHAP}}_{m,\mathrm{TPI}} = 0.62\ mM$ [29], $K^{\mathrm{PEP}}_{i,\mathrm{TPI}} = 0.5\ mM$ [32], $K^{\mathrm{3PG}}_{i,\mathrm{TPI}} = 0.51\ mM$ [32], $K^{\mathrm{2PG}}_{i,\mathrm{TPI}} = 4.1\ mM$ [32]
GADPH	$v_{\mathrm{GADPH}} = \frac{V_{max,\mathrm{GADPH}}}{1+\frac{K^{\mathrm{GA3P}}_{m,\mathrm{GADPH}}}{[\mathrm{GA3P}]}}$	$K^{\mathrm{GA3P}}_{m,\mathrm{GADPH}} = 0.149\ mM$[38]
PGM	$v_{\mathrm{PGM}} = \frac{V_{max,\mathrm{PGM}}}{1+\frac{K^{\mathrm{3PG}}_{m,\mathrm{PGM}}}{[\mathrm{3PG}]}\left(1+\frac{[\mathrm{2PG}]}{K^{\mathrm{2PG}}_{m}}\right)}$	$K^{\mathrm{3PG}}_{m,\mathrm{PGM}} = 0.4\ mM$[12], $K^{\mathrm{2PG}}_{i,\mathrm{PGM}} = 100\ mM$[12]
ENO	$v_{\mathrm{ENO}} = \frac{V_{max,\mathrm{ENO}}}{1+\frac{K^{\mathrm{2PG}}_{m,\mathrm{ENO}}}{[\mathrm{2PG}]}}$	$K^{\mathrm{2PG}}_{m,\mathrm{ENO}} = 0.12\ mM$[40]
PK	$v_{\mathrm{PK}} = \frac{V_{max,\mathrm{PK}}}{\left(1+\frac{K^{\mathrm{PEP}}_{m,\mathrm{PK}}}{[\mathrm{PEP}]}\right)\left(1+\frac{K^{\mathrm{ADP}}_{m,\mathrm{PK}}}{[\mathrm{ADP}]}\right)}$	$K^{\mathrm{PEP}}_{m,\mathrm{PK}} = 0.07\ mM$[14], $K^{\mathrm{ADP}}_{m,\mathrm{PK}} = 1.05\ mM$[14]
G6PD	$v_{\mathrm{G6PD}} = \frac{V_{max,\mathrm{G6PD}}}{1+\frac{K^{\mathrm{G6P}}_{m,\mathrm{G6PD}}}{[\mathrm{G6P}]}}$	$K^{\mathrm{G6P}}_{m,\mathrm{G6PD}} = 0.329\ mM$[11]
PGD	$v_{\mathrm{PGD}} = \frac{V_{max,\mathrm{PGD}}}{1+\frac{K^{\mathrm{6PG}}_{m,\mathrm{PGD}}}{[\mathrm{6PG}]}}$	$K^{\mathrm{6PG}}_{m,\mathrm{PGD}} = 0.157\ mM$[10]
PPE	$v_{\mathrm{PPE}} = \frac{V_{max,\mathrm{PPE}}}{1+\frac{K^{\mathrm{Ru5P}}_{m,\mathrm{PPE}}}{[\mathrm{Ru5P}]}}$	$K^{\mathrm{Ru5P}}_{m,\mathrm{PPE}} = 0.19\ mM$[59]
RPI	$v_{\mathrm{RPI}} = \frac{V_{max,\mathrm{RPI}}}{1+\frac{K^{\mathrm{Ru5P}}_{m,\mathrm{RPI}}}{[\mathrm{Ru5P}]}}$	$K^{\mathrm{Ru5P}}_{m,\mathrm{RPI}} = 0.78\ mM$[27]
TK1	$v_{\mathrm{TK1}} = \frac{V_{max,\mathrm{TK1}}}{\left(1+\frac{K^{\mathrm{X5P}}_{m,\mathrm{TK}}}{[\mathrm{X5P}]}\right)\left(1+\frac{K^{\mathrm{R5P}}_{m,\mathrm{TK}}}{[\mathrm{R5P}]}\right)}$	$K^{\mathrm{R5P}}_{m,\mathrm{TK}} = 0.33\ mM$[5], $K^{\mathrm{X5P}}_{m,\mathrm{TK}} = 0.12\ mM$[5]
TK2	$v_{\mathrm{TK2}} = \frac{V_{max,\mathrm{TK2}}}{\left(1+\frac{K^{\mathrm{X5P}}_{m,\mathrm{TK}}}{[\mathrm{X5P}]}\right)\left(1+\frac{K^{\mathrm{E4P}}_{m,\mathrm{TK}}}{[\mathrm{E4P}]}\right)}$	$K^{\mathrm{X5P}}_{m,\mathrm{TK}} = 0.12\ mM$[5], $K^{\mathrm{E4P}}_{m,\mathrm{TK}} = 0.39\ mM$[45]
TA	$v_{\mathrm{TA}} = \frac{V_{max,\mathrm{TA}}}{\left(1+\frac{K^{\mathrm{S7P}}_{m,\mathrm{TA}}}{[\mathrm{S7P}]}\right)\left(1+\frac{K^{\mathrm{GA3P}}_{m,\mathrm{TA}}}{[\mathrm{GA3P}]}\right)}$	$K^{\mathrm{S7P}}_{m,\mathrm{TA}} = 0.285\ mM$[52], $K^{\mathrm{GA3P}}_{m,\mathrm{TA}} = 0.038\ mM$[52]

Table 5 Stoichiometry of reactions considered in the model

Reaction	Stoichiometry
HK	$Glc + ATP \rightarrow G6P + ADP$
GPI	$G6P \rightleftharpoons F6P$
PFK1	$F6P + ATP \rightarrow F16BP + ADP$
ALD	$F16BP \rightarrow GA3P + DHAP$
TPI	$GA3P \rightleftharpoons DHAP$
GADPH	$GA3P + NAD^+ + P_i \rightleftharpoons 13BPG + NADH + H^+$
PGM	$3PG \rightleftharpoons 2PG$
ENO	$2PG \rightleftharpoons PEP + H_2O$
PK	$PEP + ADP \rightarrow Pyr + ATP$
G6PD	$G6P + NADP^+ \rightarrow 6PGL + NADPH + H^+$
PGD	$6PG + NADP^+ \rightarrow Ru5P + NADPH + CO_2 + H^+$
PPE	$Ru5P \rightleftharpoons X5P$
RPI	$Ru5P \rightleftharpoons R5P$
TK1	$X5P + R5P \rightleftharpoons GA3P + S7P$
TK2	$X5P + E4P \rightleftharpoons GA3P + F6P$
TA	$S7P + GA3P \rightleftharpoons E4P + F6P$

Table 6 Estimated V_{max} values in *S. cerevisiae* cells

	Scenario A	Scenario B		Scenario C	
Enzymes	V_{max}	V_{max}	Difference	V_{max}	Difference
HK	0.0175	0.0175	0.00%	0.0175	0.00%
GPI	0.0614	0.0676	+10.00%	0.0735	+19.72%
PFK1	0.0215	0.0223	+3.41%	0.0231	+7.43%
ALD	0.0140	0.0144	+3.41%	0.0150	+7.43%
TPI	0.0968	0.1003	+3.62%	0.0917	-5.27%
GADPH	0.0546	0.0557	+2.14%	0.0543	-0.53%
PGM	0.1637	0.1672	+2.14%	0.1593	-2.72%
ENO	0.0374	0.0382	+2.14%	0.0364	-2.72%
PK	0.1398	0.1428	+2.16%	0.1339	-4.23%

Table 7 Comparison of steady-state simulation and experimental results for intracellular metabolite concentrations

	S. cerevisiae cells		CHO cells	
Metabolite	In literature	Simulation (mM)	In literature	Simulation (mM)
2PG	0.420-1.100[37]	0.4190	0.005[1]	0.0050
3PG	0.100-0.260[37]	0.0998	0.040-0.048[1]	0.0400
6PG	0.100-0.300[16]	Not simulated	0.018[41]	0.0179
DHAP	0.330[31]	0.3293	0.040-0.046[1]	0.0401
E4P	Not detectable[46]	Not simulated	0.004[41]	0.0040
F16BP	1.700-4.500[16, 31]	1.6670	0.046[1]	0.0462
F6P	0.650[1]	0.6491	0.362[1]	0.3619
G6P	2.300[31]	2.2940	1.033[1]	1.0541
GA3P	0.400-1.200[37]	0.3986	0.021[6]	0.0210
Glc	1.500[53]	1.5000	2.377[1]	2.3770
PEP	$\leq$0.030[16, 31]	0.0299	0.008[1]	0.0080
Pyr	1.600[31]	1.6000	0.056[1]	0.0560
R5P	-	Not simulated	0.009[41]	0.0090
Ru5P	-	Not simulated	0.012[41]	0.0120
S7P	Not detectable[46]	Not simulated	0.068[41]	0.0676
X5P	-	Not simulated	0.018[41]	0.0180

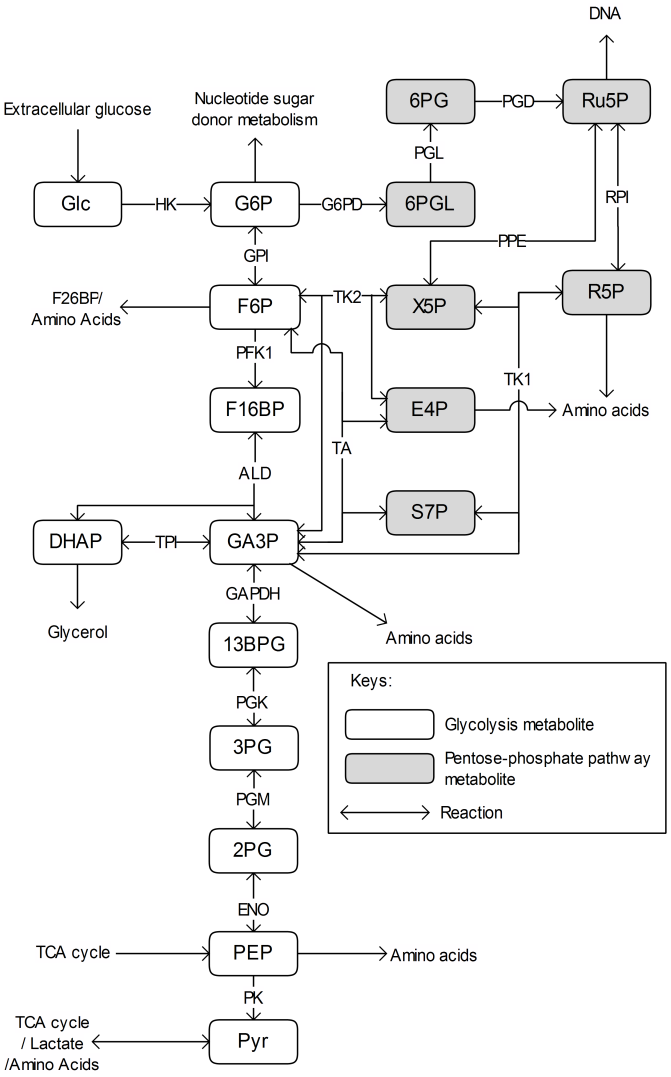

Fig. 1 Metabolic map of glycolysis and PPP for *S. cerevisiae* and CHO cells (based on KEGG and BRENDA)

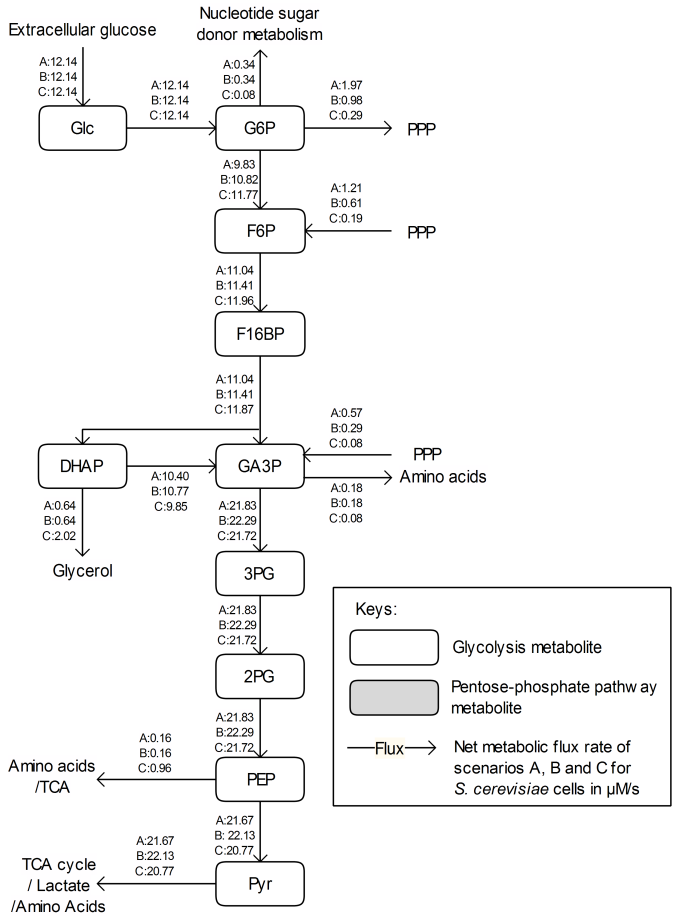

Fig. 2 Metabolic flux distribution for *S. cerevisiae* cells (calculated based on literature[20]). Arrows denote the direction of the net flux measured experimentally.

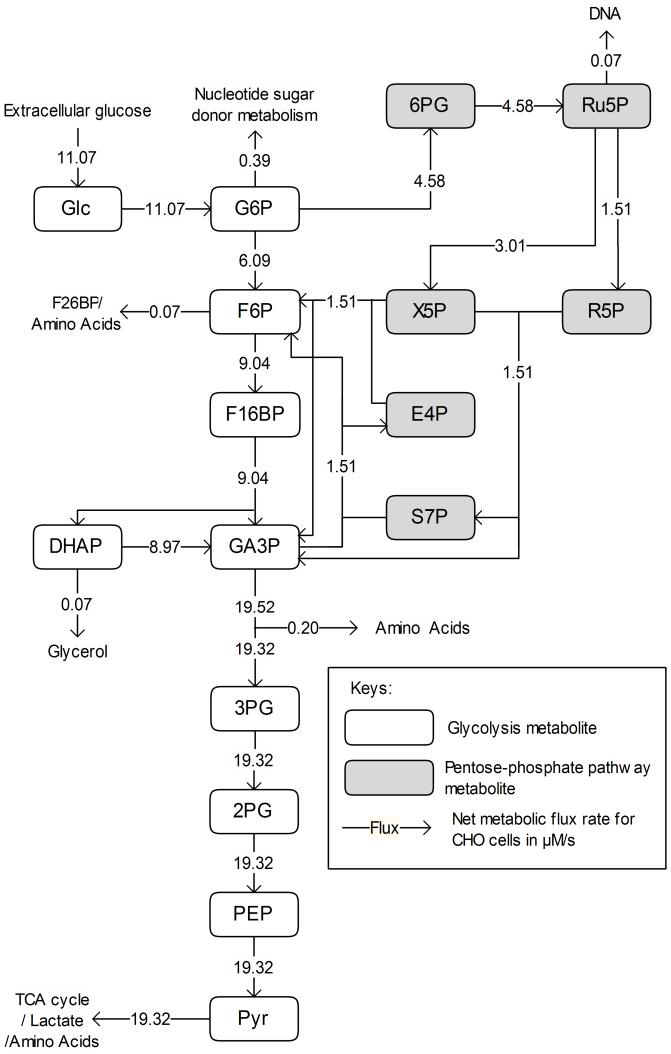

Fig. 3 Metabolic flux distribution for CHO cells (calculated based on literature[22]). Arrows denote the direction of the net flux measured experimentally.

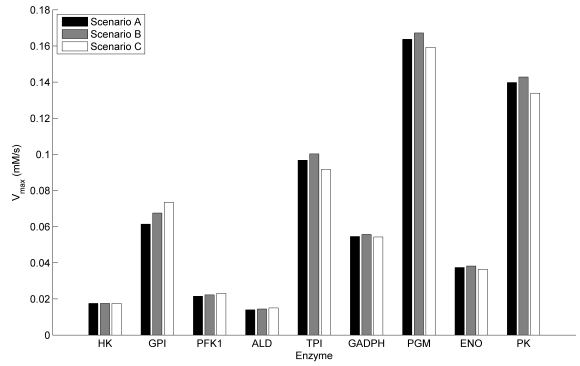

Fig. 4 Estimated V_{max} in *S. cerevisiae* cells

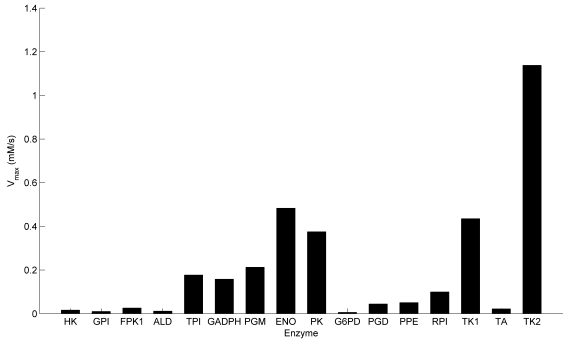

Fig. 5 Estimated V_{max} in CHO cells

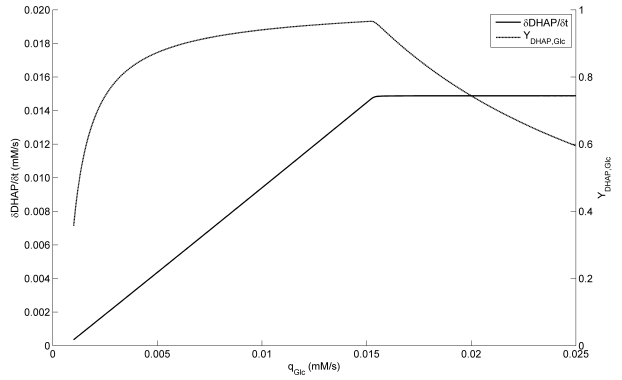

Fig. 6 DHAP accumulation rate and yield over glucose with no TPI enzyme under different glucose uptake rates